



Cite this: DOI: 10.1039/c8tc02882f

# [Cu(P<sup>^</sup>P)(N<sup>^</sup>N)][PF<sub>6</sub>] compounds with bis(phosphane) and 6-alkoxy, 6-alkylthio, 6-phenyloxy and 6-phenylthio-substituted 2,2'-bipyridine ligands for light-emitting electrochemical cells†

Murat Alkan-Zambada,<sup>a</sup> Sarah Keller,<sup>ib</sup> Laura Martínez-Sarti,<sup>ib</sup> Alessandro Prescimone,<sup>ib</sup> José M. Junquera-Hernández,<sup>ib</sup> Edwin C. Constable,<sup>ib</sup> Henk J. Bolink,<sup>ib</sup> Michele Sessolo,<sup>ib</sup>\* Enrique Ortí,<sup>ib</sup>\* and Catherine E. Housecroft<sup>ib</sup>\*<sup>a</sup>

We report a series of [Cu(P<sup>^</sup>P)(N<sup>^</sup>N)][PF<sub>6</sub>] complexes with P<sup>^</sup>P = bis(2-(diphenylphosphino)phenyl)ether (POP) or 4,5-bis(diphenylphosphino)-9,9-dimethylxanthene (xantphos) and N<sup>^</sup>N = 6-methoxy-2,2'-bipyridine (MeObpy), 6-ethoxy-2,2'-bipyridine (EtObpy), 6-phenyloxy-2,2'-bipyridine (PhObpy), 6-methylthio-2,2'-bipyridine (MeSbpy), 6-ethylthio-2,2'-bipyridine (EtSbpy) and 6-phenylthio-2,2'-bipyridine (PhSbpy). The single crystal structures of all twelve compounds have been determined and confirm chelating modes for each N<sup>^</sup>N and P<sup>^</sup>P ligand, and a distorted tetrahedral geometry for copper(i). For the xantphos-containing complexes, the asymmetrical bpy ligand is arranged with the 6-substituent lying over the xanthene 'bowl'. The compounds have been characterized in solution by <sup>1</sup>H, <sup>13</sup>C and <sup>31</sup>P NMR spectroscopies, and their photophysical and electrochemical properties are described. They are yellow emitters and solid samples show photoluminescence quantum yields in the range up to 38%, with emission lifetimes ≤10.2 μs. On going from powder to frozen Me-THF, the excited state lifetimes increase which might suggest the presence of thermally activated delayed fluorescence (TADF). All the compounds have been tested in light-emitting electrochemical cells (LECs). Bright and stable LECs are obtained with complexes containing alkoxy- or phenyloxy-substituted ligands, making this family of compounds very relevant for the future development of copper-based electroluminescent devices.

Received 12th June 2018,  
Accepted 18th July 2018

DOI: 10.1039/c8tc02882f

rsc.li/materials-c

## Introduction

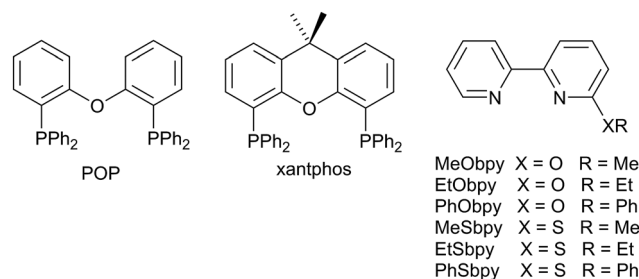
Organic light-emitting diodes (OLEDs) represent a success story of organic electronics, being already mass-produced for the latest generation of portable displays. However, due to their

level of sophistication, OLEDs are not yet fully competitive in the lighting market and in other applications where inexpensive light-sources are needed. Hence, simpler devices including light-emitting electrochemical cells (LECs) are being investigated.<sup>1–3</sup> Polymer-based LECs,<sup>4,5</sup> and LECs containing small molecules<sup>6–8</sup> or ionic transition-metal complexes (iTMCs)<sup>1,9–12</sup> as electrolumino-phores are now widely known. Among these, iTMC-based devices are among the most promising because of their high efficiencies and long lifetimes.<sup>13</sup> The most rigorously explored iTMCs are cyclometallated iridium(III) complexes, in which the large spin-orbit coupling leads to singlet-triplet mixing and harvesting of emission from both singlet and triplet states.<sup>1</sup> A disadvantage of iridium, however, is its low abundance and high cost. In contrast, copper is Earth abundant and a potential candidate for the development of dye-sensitized solar cells<sup>14</sup> and LECs. During the last few years, we<sup>15–18</sup> and others<sup>19–35</sup> have turned attention to the use of copper(i)-based complexes in LECs, in particular heteroleptic [Cu(P<sup>^</sup>P)(N<sup>^</sup>N)]<sup>+</sup>

<sup>a</sup> Department of Chemistry, University of Basel, BPR 1096, Mattenstrasse 24a, CH-4058 Basel, Switzerland. E-mail: catherine.housecroft@unibas.ch

<sup>b</sup> Instituto de Ciencia Molecular, Universidad de Valencia, Catedrático José Beltrán 2, E-46980 Paterna, Valencia, Spain. E-mail: michele.sessolo@uv.es, enrique.orti@uv.es

† Electronic supplementary information (ESI) available: Ligand and copper(i) compound syntheses, including Table S1. Fig. S1–S12: <sup>1</sup>H NMR spectra of copper(i) complexes. Fig. S13–S24: structural figures and selected bond parameters for all complexes. Table S2: crystallographic data. Fig. S25: isovalue frontier orbitals contour plots. Fig. S26–S29: additional absorption and emission spectra; Fig. S30–S33: LEC performances and electroluminescence spectra. CCDC 1562407–1562412, 1562448, 1562449, 1562453, 1562457, 1562458 and 1562460. For ESI and crystallographic data in CIF or other electronic format see DOI: 10.1039/c8tc02882f



**Scheme 1** Structures of the POP and xantphos P<sup>^</sup>P ligands and of the bpy N<sup>^</sup>N ligands substituted with alkoxy, alkylthio, phenoxy and phenylthio groups in the 6-position.

cations (P<sup>^</sup>P and N<sup>^</sup>N = chelating bis(phosphino) and diimine ligands, respectively). One of the exciting features of this family of coordination compounds is the potential for thermally activated delayed fluorescence (TADF), which accesses emission from both the triplet and singlet states.<sup>36–38</sup>

Our initial investigations of [Cu(POP)(N<sup>^</sup>N)]<sup>+</sup> cations (POP = bis(2-(diphenylphosphino)phenyl)ether) showed that the luminescence efficiency improved upon going from N<sup>^</sup>N = 2,2'-bipyridine (bpy) to 6-methyl-2,2'-bipyridine (Mebpy) and 6,6'-dimethyl-2,2'-bipyridine (Me<sub>2</sub>bpy).<sup>15,16</sup> This trend reflects the enhancement of the emission of [Cu(POP)(phen)]<sup>+</sup> observed by McMillin and coworkers upon increasing the number of substituents in the 2,9-positions of 1,10-phenanthroline (phen).<sup>39</sup> Subsequently, we extended our investigations to a series of [Cu(POP)(N<sup>^</sup>N)]<sup>+</sup> and [Cu(xantphos)(N<sup>^</sup>N)]<sup>+</sup> (xantphos = 4,5-bis(diphenylphosphino)-9,9-dimethylxanthene) emitters in which the N<sup>^</sup>N ligand was Mebpy, Me<sub>2</sub>bpy, 6-ethyl-2,2'-bipyridine (Etbpy) and 6-phenyl-2,2'-bipyridine (Phbpy). Pleasingly, a LEC with [Cu(xantphos)(Mebpy)][PF<sub>6</sub>] in the active layer had a lifetime of > 15 h (*t*<sub>1/2</sub> defined as the time for the maximum luminance, *L*<sub>max</sub>, to decay to *L*<sub>max</sub>/2); the value of *L*<sub>max</sub> was 90 cd m<sup>-2</sup>. The introduction of a second methyl substituent in [Cu(xantphos)(Me<sub>2</sub>bpy)][PF<sub>6</sub>] resulted in a shorter lifetime (0.8 h) but a brighter device (*L*<sub>max</sub> = 145 cd m<sup>-2</sup>).<sup>17</sup> Replacing the methyl group in [Cu(xantphos)(Mebpy)][PF<sub>6</sub>] by an ethyl substituent resulted in a significant gain in device lifetime but with a lower luminance (*L*<sub>max</sub> = 77 cd m<sup>-2</sup>). This series of LECs were operated under pulsed current driving.<sup>40,41</sup> The introduction of aryl groups in the 6-position of bpy proved to be detrimental to the emission behaviour.<sup>17,42</sup> We now describe the effects of incorporating alkoxy, alkylthio, phenoxy and phenylthio substituents into the 6-position of bpy (Scheme 1). While our studies were in progress, Weber *et al.* demonstrated that, for a series of [Cu(xantphos)(4,4'-R<sub>2</sub>bpy)]<sup>+</sup> complexes in which R = MeO, Me, H or NO<sub>2</sub>, the substituent with the most negative  $\sigma$ -Hammett parameter in the 4,4'-positions of the bpy ligand (4,4'-(MeO)<sub>2</sub>bpy) led to the best-performing LECs; these devices were also driven using a pulsed current mode.<sup>43</sup>

## Experimental

### General

Reactions under microwave conditions were carried out in a Biotage Initiator 8 microwave reactor. <sup>1</sup>H, <sup>13</sup>C and <sup>31</sup>P NMR

spectra were recorded at room temperature using a Bruker Avance III-600, III-500 or III-400 NMR spectrometer. <sup>1</sup>H and <sup>13</sup>C NMR chemical shifts were referenced to residual solvent peaks with respect to  $\delta(\text{TMS}) = 0$  ppm and <sup>31</sup>P NMR chemical shifts with respect to  $\delta(85\% \text{ aqueous H}_3\text{PO}_4) = 0$  ppm. Absorption and emission spectra in solution were measured using an Agilent 8453 spectrophotometer and a Shimadzu RF-5301PC spectrofluorometer, respectively. Electrospray ionization (ESI) mass spectra were recorded on a Bruker esquire 3000plus instrument. Quantum yields in CH<sub>2</sub>Cl<sub>2</sub> solution and powder were measured using a Hamamatsu absolute photoluminescence (PL) quantum yield spectrometer C11347 Quantaury-QY. Emission lifetimes and powder emission spectra were measured with a Hamamatsu Compact Fluorescence lifetime Spectrometer C11367 Quantaury-Tau, using an LED light source with  $\lambda_{\text{exc}} = 365$  nm. Lifetimes were obtained by fitting the measured data to an exponential decay using MATLAB<sup>®</sup>; a biexponential fit was used when a single exponential fit gave a poor fit. Quantum yields and PL emission spectra in thin films were recorded using a Hamamatsu absolute quantum yield C9920. Low temperature emission and lifetime experiments were performed using an LP920-KS instrument from Edinburgh Instruments; 410 nm excitation was obtained from pulsed third-harmonic radiation from a Quantel Brilliant b Nd:YAG laser equipped with a Rainbow optical parameter oscillator (OPO). The laser pulse duration was ~10 ns and the pulse frequency 10 Hz, with a typical pulse energy of 7 mJ. Detection of the spectra occurred on an iCCD camera from Andor. Single-wavelength kinetics were recorded using a photomultiplier tube.

Electrochemical measurements were made using a CH Instruments 900B potentiostat with glassy carbon, platinum wire and silver wire as the working, counter and reference electrodes, respectively. The compound for study was dissolved in HPLC grade CH<sub>2</sub>Cl<sub>2</sub> (10<sup>-4</sup> to 10<sup>-5</sup> M) containing 0.1 M [<sup>n</sup>Bu<sub>4</sub>N][PF<sub>6</sub>] as supporting electrolyte. Solutions were degassed with argon. Cp<sub>2</sub>Fe/Cp<sub>2</sub>Fe<sup>+</sup> was used as internal reference.

POP and xantphos were purchased from Acros and Fluorochem, respectively. [Cu(MeCN)<sub>4</sub>][PF<sub>6</sub>] was prepared by the published method.<sup>44</sup>

### Syntheses and characterization of copper(i) compounds

Details of syntheses, <sup>1</sup>H, <sup>13</sup>C and <sup>31</sup>P NMR characterization and assignments, electrospray mass spectrometric data, and elemental analyses are given in the ESI.<sup>†</sup>

### Crystallography

Data were collected on a Bruker Kappa Apex2 diffractometer with data reduction, solution and refinement using the programs APEX<sup>45</sup> and CRYSTALS.<sup>46</sup> Structural analysis was carried out using Mercury v. 3.5.1.<sup>47,48</sup> Crystallographic data for the complexes are given in Table S2 (ESI<sup>†</sup>). For [Cu(POP)(EtSbpy)][PF<sub>6</sub>]-Et<sub>2</sub>O, SQUEEZE<sup>49</sup> was used to treat the solvent region and electron density removed equated to one Et<sub>2</sub>O molecule per formula unit. SQUEEZE was also used for the solvent region in [Cu(xantphos)(PhSbpy)][PF<sub>6</sub>]-0.5CH<sub>2</sub>Cl<sub>2</sub> and electron density removed equated to 0.5CH<sub>2</sub>Cl<sub>2</sub> per formula unit. In 2{[Cu(POP)(PhObpy)][PF<sub>6</sub>]}-1.5CH<sub>2</sub>Cl<sub>2</sub>, half a CH<sub>2</sub>Cl<sub>2</sub> molecule per two formula units was refined and SQUEEZE

was then used to treat the solvent region; the electron density removed equated to one extra  $\text{CH}_2\text{Cl}_2$  per two formula units. In  $[\text{Cu}(\text{xantphos})(\text{EtSbpy})][\text{PF}_6] \cdot 1.5\text{Et}_2\text{O}$ , one  $\text{Et}_2\text{O}$  molecule was refined and the other  $0.5\text{Et}_2\text{O}$  was deduced based from the SQUEEZE output.

### Computational details

Density functional theory (DFT) calculations were performed for the  $[\text{Cu}(\text{P}^*\text{P})(\text{N}^*\text{N})]^+$  cations (where  $\text{P}^*\text{P} = \text{POP}$  and  $\text{xantphos}$ , and  $\text{N}^*\text{N}$  corresponds to the six bpy ligands shown in Scheme 1) using the A.03 revision of the Gaussian 16 program package.<sup>50</sup> The Becke's three-parameter B3LYP exchange–correlation functional<sup>51,52</sup> was used together with the “double- $\zeta$ ” quality def2svp basis set for C, H, N, P, S and O atoms and the “triple- $\zeta$ ” quality def2tzvp basis set for Cu atoms.<sup>53,54</sup> The D3 Grimme's dispersion term with Becke–Johnson damping was added to the B3LYP functional (B3LYP-D3) to get a better description of the intramolecular non-covalent interactions.<sup>55,56</sup> These interactions are expected to be of relevance in the determination of the molecular geometries of the studied complexes, which feature bulky POP and  $\text{xantphos}$  ligands. The geometries of all the complexes in both their singlet ground electronic state ( $S_0$ ) and their lowest-energy triplet excited state ( $T_1$ ) were optimized without imposing any symmetry restriction. The  $T_1$  state was optimized using the spin-unrestricted UB3LYP approximation with a spin multiplicity of three. The lowest-lying excited states of each complex, both singlets and triplets, were computed at the minimum-energy geometry optimized for  $S_0$  using the time-dependent DFT (TD-DFT) approach.<sup>57–59</sup> The  $S_1$  and  $T_1$  states were also optimized for a selected group of systems using the TD-DFT approach to obtain a better estimate of the adiabatic energy difference separating the minima of these two states. All the calculations were performed in the presence of the solvent ( $\text{CH}_2\text{Cl}_2$ ). Solvent effects were considered within the self-consistent reaction field (SCRf) theory using the polarized continuum model (PCM) approach.<sup>60–62</sup>

### Device preparation and characterization

LECs were prepared on top of patterned indium tin oxide (ITO,  $15 \Omega \text{ sq}^{-1}$ ) coated glass substrates previously cleaned by subsequent sonication in water with soap, deionized water and 2-propanol baths. After drying with nitrogen, the substrates were placed in a UV Ozone cleaner for 20 minutes. Prior to the deposition of the emitting layer, 80 nm thick films of poly-(3,4-ethylenedioxythiophene):poly(styrenesulfonate) (PEDOT:PSS) (CLEVIOS™ P VP AI 4083, Heraeus) were coated in order to flatten the ITO electrode and to increase its work function. The emitting layer (100 nm thick) was prepared by spin-coating a MeCN solution of the emitting compound with the addition of the ionic liquid 1-ethyl-3-methylimidazolium hexafluorophosphate  $[\text{Emim}][\text{PF}_6]$  (>98.5%, Sigma-Aldrich), in a 4 to 1 molar ratio. The devices were then transferred to an inert atmosphere glovebox (<0.1 ppm  $\text{O}_2$  and  $\text{H}_2\text{O}$ ), where the aluminium cathode (100 nm) was thermally deposited in high vacuum using an Edwards Auto500 chamber integrated in the glovebox. The thickness of all films was determined with an Ambios XP-1 profilometer.

The active area of the devices was  $4 \text{ mm}^2$ . LECs were not encapsulated and were characterized inside the glovebox at room temperature. The device lifetime was measured by applying a pulsed current and monitoring the voltage and luminance *versus* time by a True Colour Sensor MAZeT (MTCSiCT Sensor) with a Botest OLT OLED Lifetime-Test System. The electroluminescent (EL) spectra were measured using an Avantes AvaSpec-2048 Fiber Optic Spectrometer during device lifetime measurement.

## Results and discussion

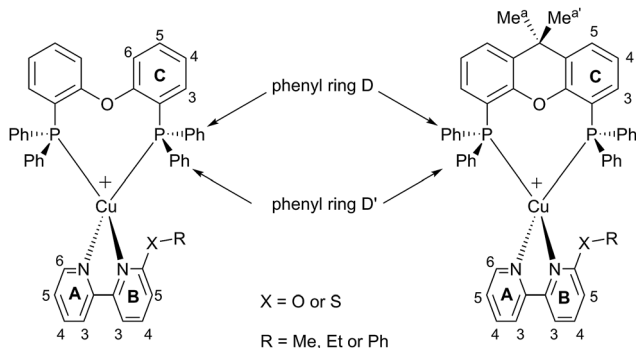
### Ligand synthesis

The compounds MeObpy, EtObpy, PhObpy, MeSbpy, EtSbpy and PhSbpy (Scheme 1) have previously been synthesized by various routes.<sup>63–67</sup> However, we found the reaction of 6-bromo-2,2'-bipyridine (prepared by Negishi coupling as described by Fang and Hanan<sup>68</sup>) with NaOR or NaSR ( $R = \text{Me}, \text{Et}, \text{Ph}$ ) under microwave conditions to be convenient. Synthetic details are given in the ESI†  $^1\text{H}$  and  $^{13}\text{C}$  NMR spectroscopic data for EtObpy<sup>63</sup> have not, to our knowledge, been reported and are given in the ESI†. The optimized reaction conditions and purification methods for the syntheses of the bipyridine ligands are summarized in Table S1 (ESI†).

### Synthesis and characterization of the $[\text{Cu}(\text{P}^*\text{P})(\text{N}^*\text{N})][\text{PF}_6]$ complexes

As previously detailed,<sup>42</sup> different strategies can be used to prepare heteroleptic  $[\text{Cu}(\text{POP})(\text{N}^*\text{N})][\text{PF}_6]$  and  $[\text{Cu}(\text{xantphos})(\text{N}^*\text{N})][\text{PF}_6]$  complexes. To ensure the formation of heteroleptic rather than homoleptic complexes, the optimized route to  $[\text{Cu}(\text{POP})(\text{N}^*\text{N})][\text{PF}_6]$  is the addition of 1–1.2 equivalents of POP to  $[\text{Cu}(\text{MeCN})_4][\text{PF}_6]$  followed, after a period of time (30 minutes to 2 hours), by addition of the  $\text{N}^*\text{N}$  ligand. Excess of POP, if added, can be removed by layer crystallization of the complex with  $\text{Et}_2\text{O}$  and subsequent washing of the microcrystalline solid with hexanes. For  $[\text{Cu}(\text{xantphos})(\text{N}^*\text{N})][\text{PF}_6]$ , a solution containing both the  $\text{N}^*\text{N}$  ligand and  $\text{xantphos}$  are added to  $[\text{Cu}(\text{MeCN})_4][\text{PF}_6]$ . These procedures were followed to afford  $[\text{Cu}(\text{POP})(\text{N}^*\text{N})][\text{PF}_6]$  and  $[\text{Cu}(\text{xantphos})(\text{N}^*\text{N})][\text{PF}_6]$  ( $\text{N}^*\text{N} = \text{MeObpy}, \text{EtObpy}, \text{PhObpy}, \text{MeSbpy}, \text{EtSbpy}$  or  $\text{PhSbpy}$ ) as yellow solids in yields ranging between 61% and 98%. The electrospray mass spectrum of each compound exhibited a peak envelope arising from the  $[\text{Cu}(\text{POP})(\text{N}^*\text{N})]^+$  or  $[\text{Cu}(\text{xantphos})(\text{N}^*\text{N})]^+$  cation (see experimental section in ESI†).

$^1\text{H}$ ,  $^{13}\text{C}$  and  $^{31}\text{P}$  NMR spectra were recorded in acetone- $d_6$  solutions, and  $^1\text{H}$  and  $^{13}\text{C}$  spectra were assigned using COSY, NOESY, HMQC and HMBC techniques; atom labelling used for NMR assignments are given in Scheme 2. Fig. 1 shows the aromatic region of the  $^1\text{H}$  NMR spectrum of  $[\text{Cu}(\text{POP})(\text{MeObpy})][\text{PF}_6]$  as a representative example (see Fig. S1, ESI† for the full spectrum) and Fig. S2–S12 (ESI†) depict the spectra of the remaining eleven complexes. In the NOESY spectrum of each  $[\text{Cu}(\text{xantphos})(\text{N}^*\text{N})][\text{PF}_6]$  compound, cross peaks between signals for  $\text{H}^a/\text{H}^{\text{C}5}$  and  $\text{H}^a'/\text{H}^{\text{C}5}$  distinguished the resonances for  $\text{H}^{\text{C}5}$  and  $\text{H}^{\text{C}3}$ .



**Scheme 2** Structures of the  $[\text{Cu}(\text{POP})(\text{N}^A\text{N}^B)]^+$  and  $[\text{Cu}(\text{xantphos})(\text{N}^A\text{N}^B)]^+$  complexes with ring and atom labelling for NMR spectroscopic data. The OPh or SPh ring is labelled E.

### Structural characterizations

X-ray quality single crystals of  $[\text{Cu}(\text{POP})(\text{MeObpy})][\text{PF}_6]$ ,  $[\text{Cu}(\text{POP})(\text{EtObpy})][\text{PF}_6]$ ,  $2\{[\text{Cu}(\text{POP})(\text{PhObpy})][\text{PF}_6]\cdot 1.5\text{CH}_2\text{Cl}_2\}$ ,  $[\text{Cu}(\text{POP})(\text{MeSbpy})][\text{PF}_6]$ ,  $[\text{Cu}(\text{POP})(\text{EtSbpy})][\text{PF}_6]\cdot \text{Et}_2\text{O}$ ,  $[\text{Cu}(\text{POP})(\text{PhSbpy})][\text{PF}_6]$ ,  $[\text{Cu}(\text{xantphos})(\text{MeObpy})][\text{PF}_6]\cdot \text{CH}_2\text{Cl}_2\cdot 0.5\text{Et}_2\text{O}$ ,  $[\text{Cu}(\text{xantphos})(\text{EtObpy})][\text{PF}_6]\cdot 0.5\text{CH}_2\text{Cl}_2\cdot 0.5\text{H}_2\text{O}$ ,  $[\text{Cu}(\text{xantphos})(\text{PhObpy})][\text{PF}_6]\cdot 3\text{CH}_2\text{Cl}_2$ ,  $[\text{Cu}(\text{xantphos})(\text{MeSbpy})][\text{PF}_6]\cdot 0.5\text{CH}_2\text{Cl}_2\cdot 0.5\text{Et}_2\text{O}$ ,  $[\text{Cu}(\text{xantphos})(\text{EtSbpy})][\text{PF}_6]\cdot 1.5\text{Et}_2\text{O}$  and  $[\text{Cu}(\text{xantphos})(\text{PhSbpy})][\text{PF}_6]\cdot 0.5\text{CH}_2\text{Cl}_2$  were grown by slow diffusion of  $\text{Et}_2\text{O}$  into  $\text{CH}_2\text{Cl}_2$  solutions of the complexes. Crystallographic data for the compounds are summarized in Table S2 (ESI<sup>†</sup>). The structure determinations confirmed the expected chelating mode of each  $\text{N}^A\text{N}^B$  and  $\text{P}^A\text{P}^B$  ligand, and the distorted tetrahedral coordination geometry of each copper(II) centre. The structures are shown in ORTEP style in Fig. S13–S24 (ESI<sup>†</sup>), and selected bond parameters are given in the figure captions. The six POP-containing compounds exhibit similar gross structural features, as do members of the xantphos series. The Cu–P and Cu–N bond distances in the twelve compounds lie in the expected ranges 2.2259(6)–2.2913(7) and 2.026(4)–2.138(2) Å, respectively. Table 1 gives values of the P–Cu–P and N–Cu–N angles, the angles between the PCuP and NCuN planes, and the bpy N–C–C–N torsion angles, and also includes data for  $[\text{Cu}(\text{POP})(\text{bpy})][\text{PF}_6]^{15}$  and  $[\text{Cu}(\text{xantphos})(\text{bpy})][\text{PF}_6]^{69}$  as benchmarks. The chelate angle of the bpy ligands is essentially fixed (Table 1). There is only a small variation in the xantphos P–Cu–P chelate angle, and the range of 113.29(3)–115.71(2)° compares to 113.816(14)° in  $[\text{Cu}(\text{xantphos})(\text{bpy})]^+$ . In contrast, the more flexible POP ligand, in which the P···P distance is

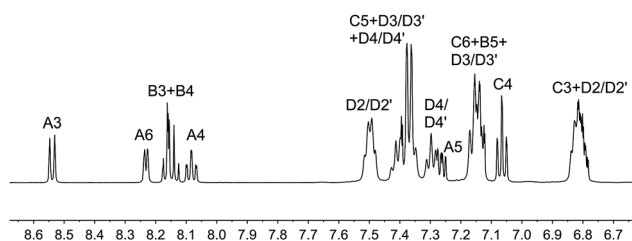


**Fig. 1** Part of the 500 MHz  $^1\text{H}$  NMR spectrum of  $[\text{Cu}(\text{POP})(\text{MeObpy})][\text{PF}_6]$  in acetone- $d_6$ . Chemical shifts in  $\delta/\text{ppm}$ . See Fig. S1 (ESI<sup>†</sup>) for the complete spectrum. Atom labels are defined in Scheme 2.

variable, exhibits a range of P–Cu–P bond angles from 108.64(3) to 118.99(3)°, compared to 115.00(3)° in  $[\text{Cu}(\text{POP})(\text{bpy})]^+$ . In most cases, the angle between the PCuP and NCuN planes is close to (or is) 90°. The values of 79.6 and 74.9° observed in the benchmark  $[\text{Cu}(\text{xantphos})(\text{bpy})]^+$  and one independent  $[\text{Cu}(\text{POP})(\text{PhObpy})]^+$  cation, respectively, are associated with significant twisting of the bpy backbone (torsion angles of 20.5(2) and 15.9(3)°, respectively).

For each of the xantphos-containing complexes, the asymmetrical bpy ligand is oriented with the 6-substituent lying over the xanthene 'bowl' (Fig. 2 and 3). We have previously reported that in solution,  $[\text{Cu}(\text{xantphos})(\text{N}^A\text{N}^B)]^+$  complexes may exist as a mixture of conformers which interconvert through inversion of the xanthene bowl-shaped unit, and that a preference for a given orientation is influenced by steric factors.<sup>17,42</sup> In the solid-state structure of  $[\text{Cu}(\text{xantphos})(6\text{-CF}_3\text{bpy})][\text{PF}_6]$  (6- $\text{CF}_3\text{bpy}$  = 6-trifluoromethyl-2,2'-bipyridine), the 6- $\text{CF}_3\text{bpy}$  ligand is orientationally disordered with the  $\text{CF}_3$  group facing the xanthene unit (modelled with 75% occupancy) or away from it (25% occupancy).<sup>69</sup>

In contrast to the POP-containing compounds, each of the complexes with xantphos features a face-to-face  $\pi$ -stacking interaction between phenyl rings of the two  $\text{PPh}_2$  units. Fig. 3 shows the similarity between the orientations of the phenyl rings in all six  $[\text{Cu}(\text{xantphos})(\text{N}^A\text{N}^B)]^+$  cations. In  $[\text{Cu}(\text{xantphos})(\text{MeObpy})]^+$ , the angle between the planes of the  $\pi$ -stacked phenyl rings is 7.1°, the centroid···plane distance is 3.66 Å and the centroid···centroid distance is 3.82 Å. These parameters are 6.0°, 3.70 Å and 3.80 Å for  $[\text{Cu}(\text{xantphos})(\text{EtObpy})]^+$ , 10.0°, 3.73 Å and 3.83 Å for  $[\text{Cu}(\text{xantphos})(\text{PhObpy})]^+$ , 4.8°, 3.72 Å and 3.80 Å for  $[\text{Cu}(\text{xantphos})(\text{MeSbpy})]^+$ , 6.5°, 3.65 Å and 3.72 Å for  $[\text{Cu}(\text{xantphos})(\text{EtSbpy})]^+$  and 6.2°, 3.65 Å and 4.00 Å for  $[\text{Cu}(\text{xantphos})(\text{PhSbpy})]^+$ . Thus, all these  $\pi$ -stacking interactions are efficient.<sup>70</sup>

Intramolecular  $\pi$ -stacking features are only present in some of the  $[\text{Cu}(\text{POP})(\text{N}^A\text{N}^B)]^+$  cations, and the aromatic rings involved vary. Stacking of one phenyl ring of a  $\text{PPh}_2$  unit and one arene ring of the POP backbone is seen in  $[\text{Cu}(\text{POP})(\text{MeObpy})]^+$ ,  $[\text{Cu}(\text{POP})(\text{EtObpy})]^+$  and  $[\text{Cu}(\text{POP})(\text{EtSbpy})]^+$ , but the interactions are not ideal, with angles between the ring planes of 19.4, 23.5 and 16.6°, respectively. In contrast,  $[\text{Cu}(\text{POP})(\text{MeSbpy})]^+$  and one of the crystallographically independent  $[\text{Cu}(\text{POP})(\text{PhObpy})]^+$  cations exhibit  $\pi$ -stacking between one  $\text{PPh}_2$  phenyl ring and one ring of the bpy unit (centroid···centroid separations of 3.79 and 3.61 Å, respectively, and centroid···ring plane distances of 3.56 and 3.40 Å, respectively). No intramolecular  $\pi$ -stacking contacts are present in  $[\text{Cu}(\text{POP})(\text{PhSbpy})]^+$  and the second  $[\text{Cu}(\text{POP})(\text{PhObpy})]^+$  cation. The variation presumably arises from the flexibility of the POP ligand, and is in sharp contrast to the consistency of the phenyl···phenyl interactions among the xantphos-containing compounds (Fig. 3).

As with the O-atom of the POP and xantphos ligands, the O- and S-atoms of the 6-substituents of the bpy ligands are potential donors, but all Cu···O and Cu···S separations are too long to be considered as meaningful interactions. For POP, Cu···O separations are in the range 2.977(2)–3.257(2) Å, and for

**Table 1** Comparison of important structural parameters in the cations of the  $[\text{Cu}(\text{P}^{\wedge}\text{P})(\text{N}^{\wedge}\text{N})][\text{PF}_6]$  compounds. Reference  $[\text{Cu}(\text{P}^{\wedge}\text{P})(\text{bpy})][\text{PF}_6]$  complexes are included for comparison

Cation	P–Cu–P chelating angle/ $^{\circ}$	N–Cu–N chelating angle/ $^{\circ}$	P...P distance/ $\text{\AA}$	Angle between PCuP and NCuN planes/ $^{\circ}$	N–C–N torsion angle/ $^{\circ}$
$[\text{Cu}(\text{POP})(\text{bpy})]^+{}^a$	115.00(3)	79.66(7)	3.790(1)	88.5	–2.8(3)
$[\text{Cu}(\text{POP})(\text{MeObpy})]^+$	113.83(5)	79.49(17)	3.779(1)	89.7	2.2(7)
$[\text{Cu}(\text{POP})(\text{EtObpy})]^+$	116.48(2)	79.65(7)	3.8236(7)	87.8	–0.9(3)
$[\text{Cu}(\text{POP})(\text{PhObpy})]^+{}^b$	110.83(3)	79.43(8)	3.7039(9)	74.9	15.9(3)
	108.64(3)	79.04(9)	3.6755(9)	86.7	–2.7(3)
$[\text{Cu}(\text{POP})(\text{MeSbpy})]^+$	118.99(3)	78.09(9)	3.894(1)	90.0	–3.6(4)
$[\text{Cu}(\text{POP})(\text{EtSbpy})]^+$	113.86(7)	79.8(2)	3.778(2)	84.9	4.1(8)
$[\text{Cu}(\text{POP})(\text{PhSbpy})]^+$	112.49(2)	78.86(7)	3.7844(8)	87.5	–3.2(3)
$[\text{Cu}(\text{xantphos})(\text{bpy})]^+{}^c$	113.816(14)	79.32(5)	3.8010(5)	79.6	20.5(2)
$[\text{Cu}(\text{xantphos})(\text{MeObpy})]^+$	114.42(4)	79.67(13)	3.778(1)	87.2	–1.6(5)
$[\text{Cu}(\text{xantphos})(\text{EtObpy})]^+$	114.15(4)	79.91(17)	3.768(1)	88.8	0.4(7)
$[\text{Cu}(\text{xantphos})(\text{PhObpy})]^+$	113.29(3)	78.76(11)	3.7746(9)	89.4	0.8(5)
$[\text{Cu}(\text{xantphos})(\text{MeSbpy})]^+$	113.33(3)	79.70(11)	3.771(1)	87.4	1.2(5)
$[\text{Cu}(\text{xantphos})(\text{EtSbpy})]^+$	113.65(3)	79.48(9)	3.7844(9)	88.6	2.8(4)
$[\text{Cu}(\text{xantphos})(\text{PhSbpy})]^+$	115.71(2)	79.40(8)	3.8256(8)	86.8	–0.0(3)

<sup>a</sup> Data for  $[\text{Cu}(\text{POP})(\text{bpy})][\text{PF}_6]\cdot\text{CHCl}_3$ .<sup>15</sup> <sup>b</sup> Two crystallographically independent cations. <sup>c</sup> Data for  $[\text{Cu}(\text{xantphos})(\text{bpy})][\text{PF}_6]$ .<sup>69</sup>

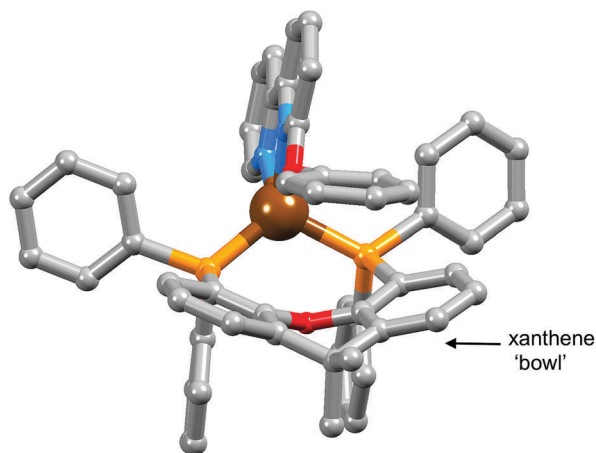


**Fig. 2** Structure of the  $[\text{Cu}(\text{xantphos})(\text{PhObpy})]^+$  cation (H atoms omitted for clarity) showing the orientation of the 6-substituted bpy ligand with respect to the xanthene 'bowl' of the xantphos ligand.

xantphos the range is 3.225(4)–3.257(2)  $\text{\AA}$ . For the OR substituents, Cu...O separations are between 3.035(5) and 3.204(2)  $\text{\AA}$ , and for the sulfur-containing ligands, the Cu...S separations lie in the range 3.201(1)–3.2655(8)  $\text{\AA}$ .

### Electrochemistry

Cyclic voltammetry was used to investigate the redox activity of the copper(i) complexes in  $\text{CH}_2\text{Cl}_2$  solution. Each complex showed a quasi-reversible copper-based oxidation (Table 2) and the range of values (+0.74 to +0.86 V) is similar to other  $[\text{Cu}(\text{POP})(\text{N}^{\wedge}\text{N})][\text{PF}_6]$  and  $[\text{Cu}(\text{xantphos})(\text{N}^{\wedge}\text{N})][\text{PF}_6]$  complexes in which the  $\text{N}^{\wedge}\text{N}$  ligand is a 6-substituted bpy.<sup>17,42</sup> Ligand-based reduction processes within the solvent accessible window were poorly defined. The  $\text{Cu}^+/\text{Cu}^{2+}$  processes are all at higher potentials than those of the benchmark compounds  $[\text{Cu}(\text{POP})(\text{bpy})][\text{PF}_6]$  (+0.72 V) and  $[\text{Cu}(\text{xantphos})(\text{bpy})][\text{PF}_6]$  (+0.76 V),<sup>69</sup> indicating that the substituents in the 6-position of the bpy ligand render the

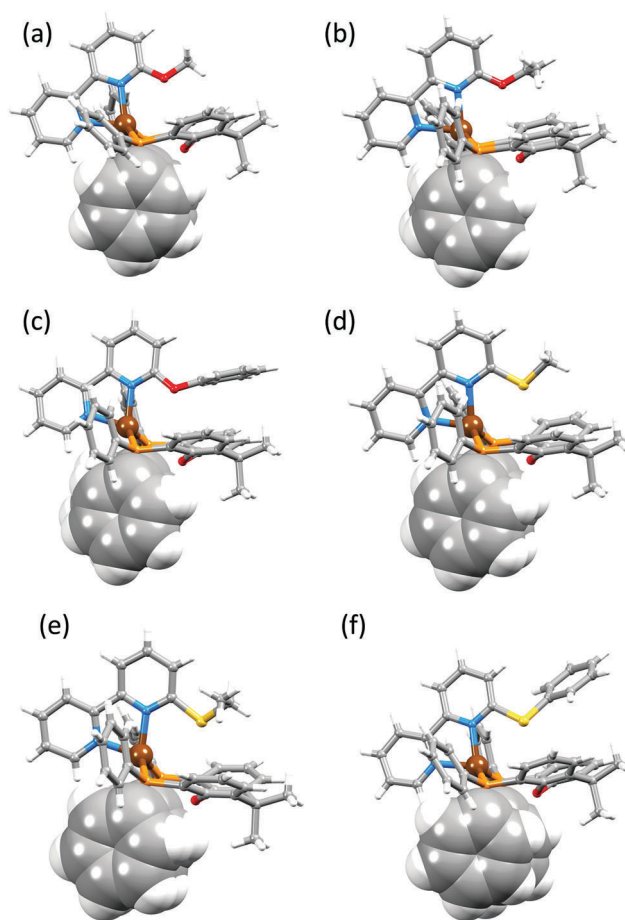


**Fig. 3** The structures of the xantphos-containing cations showing face-to-face  $\pi$ -stacking between phenyl rings of two  $\text{PPh}_2$  units: (a)  $[\text{Cu}(\text{xantphos})(\text{MeObpy})]^+$ , (b)  $[\text{Cu}(\text{xantphos})(\text{EtObpy})]^+$ , (c)  $[\text{Cu}(\text{xantphos})(\text{PhObpy})]^+$ , (d)  $[\text{Cu}(\text{xantphos})(\text{MeSbpy})]^+$ , (e)  $[\text{Cu}(\text{xantphos})(\text{EtSbpy})]^+$ , (f)  $[\text{Cu}(\text{xantphos})(\text{PhSbpy})]^+$ .

$\text{Cu}^+/\text{Cu}^{2+}$  process more positive by stabilizing the tetrahedral geometry of the copper(i) cation.

## DFT calculations

The geometries of all the  $[\text{Cu}(\text{P}^{\wedge}\text{P})(\text{N}^{\wedge}\text{N})]^+$  cations in their electronic ground state ( $S_0$ ) were optimized without imposing any symmetry restriction at the DFT B3LYP-D3/(def2svp + def2tzvp) level in the presence of solvent ( $\text{CH}_2\text{Cl}_2$ ). A selection of calculated geometrical parameters regarding the coordination sphere of Cu(I) is given in Table S3 (ESI<sup>†</sup>). As previously reported for related Cu-ITMCs,<sup>71</sup> the theoretical approach employed here reproduces the distorted tetrahedral structures observed in the single crystal X-ray diffraction with accuracies of 0.04 Å for the Cu–P and Cu–N bond distances and of 4° for the P–Cu–P and N–Cu–N chelating angles.

The geometry of the first triplet excited state ( $T_1$ ) was also optimized at the UB3LYP-D3 level for all the  $[\text{Cu}(\text{P}^{\wedge}\text{P})(\text{N}^{\wedge}\text{N})]^+$  cations (Table S3, ESI<sup>†</sup>). As discussed below, the  $T_1$  state implies a charge transfer from a d orbital of the Cu atom ( $d^{10}$ ) to a molecular orbital centered on the bpy ligand. Consequently, the metal atom features a partial oxidation and deviates from the tetrahedral geometry obtained for  $S_0$ , tending to adopt the square-planar coordination sphere expected for four-fold coordinated  $d^9$  Cu complexes. The angle defined by the PCuP and NCuN planes has a value of 90° for a perfect tetrahedral structure and can be used as an estimation of the deviation from the orthogonal disposition of the  $\text{P}^{\wedge}\text{P}$  and the  $\text{N}^{\wedge}\text{N}$  ligands. The values computed for this angle are collected in Table 3, which also includes those previously reported for the reference complexes  $[\text{Cu}(\text{POP})(\text{bpy})]^+$  and  $[\text{Cu}(\text{xantphos})(\text{bpy})]^+$ ,<sup>71</sup> and give us information about the extent of the flattening experienced by the complex upon excitation from  $S_0$  to  $T_1$ . The angle is calculated to be greater than 80° for all the complexes in the  $S_0$  state, being slightly higher and more uniform for the xantphos-containing complexes (86.6–89.7°) than for the POP complexes (80.4–86.0°) due to the higher rigidity of the xantphos ligand. The values for the xantphos complexes are indeed very similar to the experimental X-ray values (86.8–89.4°) reported in Table 1. In the excited  $T_1$  state, the angle formed by the PCuP and NCuN planes drastically changes showing a reduction in the range 20–24° for the two families of complexes. This reduction is significantly smaller than that found for the

Table 2 Cyclic voltammetry data for  $[\text{Cu}(\text{P}^{\wedge}\text{P})(\text{N}^{\wedge}\text{N})][\text{PF}_6]$  complexes in  $\text{CH}_2\text{Cl}_2$  (vs.  $\text{Fc}^+/\text{Fc}$ ,  $[\text{t}^{\text{Bu}}\text{Bu}_4\text{N}][\text{PF}_6]$  as supporting electrolyte, scan rate = 0.1 V s<sup>-1</sup>). Data for  $[\text{Cu}(\text{P}^{\wedge}\text{P})(\text{bpy})][\text{PF}_6]$  are included for comparison

Compound	$E_{1/2}^{\text{ox}}/\text{V}$	$(E_{\text{pc}} - E_{\text{pa}})/\text{mV}$
$[\text{Cu}(\text{POP})(\text{MeObpy})][\text{PF}_6]$	+0.74	90
$[\text{Cu}(\text{POP})(\text{EtObpy})][\text{PF}_6]$	+0.76	100
$[\text{Cu}(\text{POP})(\text{PhObpy})][\text{PF}_6]$	+0.80	130
$[\text{Cu}(\text{POP})(\text{MeSbpy})][\text{PF}_6]$	+0.84	110
$[\text{Cu}(\text{POP})(\text{EtSbpy})][\text{PF}_6]$	+0.84	100
$[\text{Cu}(\text{POP})(\text{PhSbpy})][\text{PF}_6]$	+0.84	100
$[\text{Cu}(\text{POP})(\text{bpy})][\text{PF}_6]^a$	+0.72	110
$[\text{Cu}(\text{xantphos})(\text{MeObpy})][\text{PF}_6]$	+0.81	90
$[\text{Cu}(\text{xantphos})(\text{EtObpy})][\text{PF}_6]$	+0.82	110
$[\text{Cu}(\text{xantphos})(\text{PhObpy})][\text{PF}_6]$	+0.86	110
$[\text{Cu}(\text{xantphos})(\text{MeSbpy})][\text{PF}_6]$	+0.80	100
$[\text{Cu}(\text{xantphos})(\text{EtSbpy})][\text{PF}_6]$	+0.82	100
$[\text{Cu}(\text{xantphos})(\text{PhSbpy})][\text{PF}_6]$	+0.80	110
$[\text{Cu}(\text{xantphos})(\text{bpy})][\text{PF}_6]^a$	+0.76	110

<sup>a</sup> Values from ref. 69.

Table 3 Angles defined by the PCuP and NCuN planes computed for both  $S_0$  and  $T_1$  states, and frontier molecular orbital energies calculated for  $S_0$  for all the  $[\text{Cu}(\text{P}^{\wedge}\text{P})(\text{N}^{\wedge}\text{N})]^+$  complexes at the B3LYP-D3/(def2svp + def2tzvp) level

Compound	Angle $S_0/^\circ$	Angle $T_1/^\circ$	HOMO/eV	LUMO/eV
$[\text{Cu}(\text{POP})(\text{bpy})]^+{}^a$	80.4	59.7	-5.94	-2.46
$[\text{Cu}(\text{POP})(\text{MeObpy})]^+{}^a$	81.1	60.7	-5.87	-2.46
$[\text{Cu}(\text{POP})(\text{EtObpy})]^+$	82.6	60.8	-5.90	-2.47
$[\text{Cu}(\text{POP})(\text{PhObpy})]^+$	86.0	63.8	-5.92	-2.55
$[\text{Cu}(\text{POP})(\text{MeSbpy})]^+$	82.0	62.1	-5.94	-2.52
$[\text{Cu}(\text{POP})(\text{EtSbpy})]^+$	82.3	62.8	-5.93	-2.52
$[\text{Cu}(\text{POP})(\text{PhSbpy})]^+$	84.4	65.3	-5.98	-2.55
$[\text{Cu}(\text{xantphos})(\text{bpy})]^+$	86.9	57.5	-6.00	-2.56
$[\text{Cu}(\text{xantphos})(\text{MeObpy})]^+$	87.8	61.0	-5.92	-2.53
$[\text{Cu}(\text{xantphos})(\text{EtObpy})]^+$	88.8	65.0	-5.91	-2.52
$[\text{Cu}(\text{xantphos})(\text{PhObpy})]^+$	89.7	65.6	-5.93	-2.57
$[\text{Cu}(\text{xantphos})(\text{MeSbpy})]^+$	86.6	64.1	-5.90	-2.53
$[\text{Cu}(\text{xantphos})(\text{EtSbpy})]^+$	88.0	65.0	-5.93	-2.55
$[\text{Cu}(\text{xantphos})(\text{PhSbpy})]^+$	89.4	69.4	-5.92	-2.52

<sup>a</sup> Values from ref. 71.

reference  $[\text{Cu}(\text{xantphos})(\text{bpy})]^+$  complex ( $\sim 30^\circ$ ), and is similar to that calculated for the  $[\text{Cu}(\text{xantphos})(6\text{-Mebpy})]^+$  complex, for which a decrease of 21° (from 88.3 to 67.3°) is obtained. This reflects the fact that the geometrical flattening of the complex is hindered by the presence of substituents in 6-position of the bpy ligand in agreement with the results reported in previous works<sup>69,71</sup> and fully supports the trends observed experimentally for the  $\text{Cu}^+/\text{Cu}^{2+}$  processes (Table 2). Substituents in the 6-position impede the movement of the ligand towards a more planar cation geometry thus limiting the distortion from the tetrahedral structure on going from  $S_0$  to  $T_1$ . The distortion is indeed slightly smaller for the complexes bearing the bulkier PhO- and PhS-groups (see Table 3). As discussed below, this limited geometry relaxation in  $T_1$  induces a blue shift of the emission with respect to that expected based on electronic considerations.

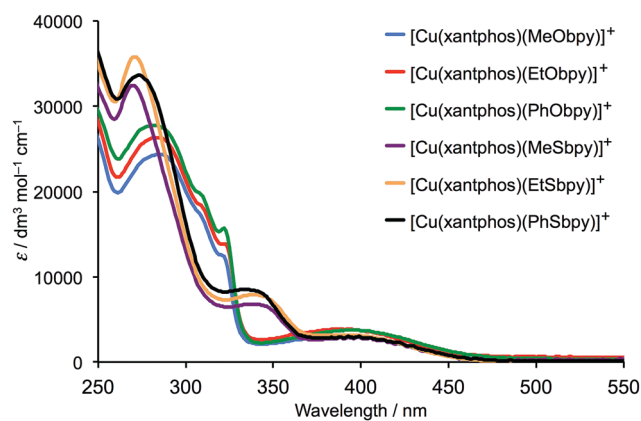
The energies calculated for the highest-occupied (HOMO) and lowest-unoccupied molecular orbital (LUMO) of the studied complexes are summarized in Table 3, and the isovalue contour plots for the HOMO and LUMO of two representative examples are shown in Fig. S25 (ESI<sup>†</sup>). As previously reported for this type of complex,<sup>7,15,17,69,71</sup> the HOMO is mainly centred over the metal and the phosphorus atoms, with small contributions of the phenyl rings, and the LUMO is exclusively located on the  $\text{N}^{\wedge}\text{N}$  ligand. As the HOMO is situated on a region that undergoes no structural change along the series, its energy only features small variations within the two family of complexes, in good agreement with the similar values registered for the  $\text{Cu}^+/\text{Cu}^{2+}$  processes (Table 2). The LUMO shows almost no contribution of the substituents in 6-position of the bpy ligand and its energy lies in a range of 0.1 eV. The HOMO–LUMO energy gap therefore oscillates between 3.36 and 3.43 eV, and it is expected that the excited states described by the LUMO←HOMO monoexcitation appear at similar energies for all the complexes studied.

## Photophysical properties

The absorption spectroscopic data for  $\text{CH}_2\text{Cl}_2$  solutions of the  $[\text{Cu}(\text{P}^{\wedge}\text{P})(\text{N}^{\wedge}\text{N})][\text{PF}_6]$  complexes are given in Table 4, and Fig. 4

Table 4 Absorption spectroscopic data for CH<sub>2</sub>Cl<sub>2</sub> solutions of the [Cu(P<sup>^</sup>P)(N<sup>^</sup>N)][PF<sub>6</sub>]<sub>2</sub> complexes

Compound	$\lambda_{\max}/\text{nm}$ ( $\epsilon/(\text{dm}^3 \text{ mol}^{-1} \text{ cm}^{-1})$ )	
	Ligand-based	MLCT
[Cu(POP)(MeObpy)][PF <sub>6</sub> ]	306 (22 600)	393 (3300)
[Cu(POP)(EtObpy)][PF <sub>6</sub> ]	305 (20 600)	393 (3300)
[Cu(POP)(PhObpy)][PF <sub>6</sub> ]	307 (23 500)	398 (3100)
[Cu(POP)(MeSbpy)][PF <sub>6</sub> ]	268 (27 000), 333sh (9800)	398 (2600)
[Cu(POP)(EtSbpy)][PF <sub>6</sub> ]	269 (25 000), 320sh (9584)	393 (2800)
[Cu(POP)(PhSbpy)][PF <sub>6</sub> ]	267 (28 200), 330sh (10 900)	399 (2833)
[Cu(xantphos)(MeObpy)][PF <sub>6</sub> ]	285 (24 400), 307sh (17 700), 326sh (11 800)	389 (3100)
[Cu(xantphos)(EtObpy)][PF <sub>6</sub> ]	284 (26 300), 305sh (19 000), 322sh (13 900)	388 (3900)
[Cu(xantphos)(PhObpy)][PF <sub>6</sub> ]	282 (27 700), 307sh (20 000), 322sh (15 700)	393 (3800)
[Cu(xantphos)(MeSbpy)][PF <sub>6</sub> ]	270 (32 400), 336 (6800)	393 (3000)
[Cu(xantphos)(EtSbpy)][PF <sub>6</sub> ]	271 (35 800), 338 (7900)	391 (3200)
[Cu(xantphos)(PhSbpy)][PF <sub>6</sub> ]	273 (33 700), 333 (8500)	393 (3000)

Fig. 4 Absorption spectra of CH<sub>2</sub>Cl<sub>2</sub> solutions of [Cu(xantphos)-(N<sup>^</sup>N)][PF<sub>6</sub>]<sub>2</sub> complexes (concentration = 2.5 × 10<sup>-5</sup> mol dm<sup>-3</sup>).

compares the spectra of the compounds containing xantphos. Fig. S26 (ESI<sup>†</sup>) shows the spectra of the POP-containing complexes. The intense high-energy absorptions between 250 and 350 nm are assigned to ligand-based  $\pi \rightarrow \pi^*$  and  $n \rightarrow \pi^*$  transitions, and the shift to lower energy on replacing oxygen by sulfur is consistent with the trends observed in 2-substituted pyridines, for example on going from 2-methoxypyridine to 2-methylthiopyridine.<sup>72</sup> The broad absorption around 390 nm arises from a metal-to-ligand charge transfer (MLCT). The position of this band is essentially independent of the 6-substituent and of the P<sup>^</sup>P ligand. However, the maxima of the MLCT bands of the complexes with 6-OR or 6-SR substituents are all at lower energies than the corresponding complexes with bpy, namely [Cu(POP)(bpy)][PF<sub>6</sub>]<sub>2</sub> with  $\lambda_{\max} = 388$  nm and [Cu(xantphos)(bpy)][PF<sub>6</sub>]<sub>2</sub> with  $\lambda_{\max} = 383$  nm.<sup>69</sup> The OR/SR substituents lead to a smaller HOMO–LUMO gap by stabilizing the LUMO which is mainly located on the bpy ligand (Fig. S25, ESI<sup>†</sup>).

To gain greater insight into the nature of the low-lying electronic states, the lowest-energy singlet and triplet excited states were calculated using the time-dependent DFT (TD-DFT) approach. The vertical B3LYP-D3/(def2svp + def2tzvp) excitation energies computed for the S<sub>1</sub> and T<sub>1</sub> states at the optimized geometry of S<sub>0</sub> are collected in Table 5. In all cases, the main

Table 5 Vertical excitation energies calculated at the TD-DFT B3LYP-D3/(def2svp + def2tzvp) level for the lowest singlet (S<sub>1</sub>) and triplet (T<sub>1</sub>) excited states of complexes [Cu(P<sup>^</sup>P)(N<sup>^</sup>N)]<sup>+</sup> in CH<sub>2</sub>Cl<sub>2</sub> solution. S<sub>0</sub> → S<sub>1</sub> oscillator strengths (*f*) are given within parentheses

Compound	S <sub>1</sub> /eV	T <sub>1</sub> /eV
[Cu(POP)(MeObpy)] <sup>+</sup>	2.78 (0.09)	2.52
[Cu(POP)(EtObpy)] <sup>+</sup>	2.79 (0.09)	2.54
[Cu(POP)(PhObpy)] <sup>+</sup>	2.75 (0.08)	2.51
[Cu(POP)(MeSbpy)] <sup>+</sup>	2.77 (0.11)	2.55
[Cu(POP)(EtSbpy)] <sup>+</sup>	2.77 (0.10)	2.55
[Cu(POP)(PhSbpy)] <sup>+</sup>	2.77 (0.10)	2.57
[Cu(xantphos)(MeObpy)] <sup>+</sup>	2.77 (0.07)	2.52
[Cu(xantphos)(EtObpy)] <sup>+</sup>	2.77 (0.07)	2.53
[Cu(xantphos)(PhObpy)] <sup>+</sup>	2.75 (0.06)	2.50
[Cu(xantphos)(MeSbpy)] <sup>+</sup>	2.73 (0.08)	2.50
[Cu(xantphos)(EtSbpy)] <sup>+</sup>	2.76 (0.08)	2.53
[Cu(xantphos)(PhSbpy)] <sup>+</sup>	2.75 (0.07)	2.53

contribution (>95%) to both states comes from the HOMO → LUMO monoexcitation. This excitation implies an electron transfer from the Cu(P<sup>^</sup>P) environment to the bpy ligand, and therefore confirms the MLCT character of the S<sub>1</sub> and T<sub>1</sub> states. The transition to S<sub>1</sub> accounts for the low-energy band observed in the 400 nm region in the absorption spectra (Fig. 4), as no other singlet state with relevant oscillator strength is calculated in this energy range. The almost identical energies predicted for the S<sub>0</sub> → S<sub>1</sub> transition are in good agreement with the very similar values calculated for the HOMO–LUMO gaps, and reproduce the trend observed experimentally for the absorption maxima of the MLCT band, which lie in a narrow range of only 11 nm for the entire set of complexes (Table 4).

Photoluminescence (PL) spectra of the complexes were recorded for deaerated CH<sub>2</sub>Cl<sub>2</sub> solutions and powder samples. Table 6 presents PL maxima ( $\lambda_{\text{em}}^{\text{max}}$ ), photoluminescence quantum yields (PLQY) and PL lifetimes ( $\tau$ ), and includes previously reported data for [Cu(POP)(bpy)][PF<sub>6</sub>]<sub>2</sub> and [Cu(xantphos)(bpy)][PF<sub>6</sub>]<sub>2</sub><sup>69</sup> for comparison. The PL spectra of the xantphos- and POP-containing complexes in solution are shown in Fig. 5 and Fig. S27 (ESI<sup>†</sup>), respectively. All compounds are yellow emitters both in solution and in the solid state, with emissions in solution being very weak (PLQY ≤ 1%). The emission bands are broad and exhibit two maxima around 610 and 635 nm (Table 6), which are similar to those of

Table 6 Photoluminescence characterization for solutions, powder, frozen solution at 77 K and thin films of the  $[\text{Cu}(\text{N}^{\wedge}\text{N})(\text{P}^{\wedge}\text{P})][\text{PF}_6]$  complexes

Compound	Solution	Solution			Powder			Solution at 77 K			Film
		$\lambda_{\text{em}}^{\text{max}}/\text{nm}$	PLQY (deaerated)/%	$\tau$ (deaerated)/ns	$\lambda_{\text{em}}^{\text{max}}/\text{nm}$	PLQY/%	$\tau/\mu\text{s}$	$\lambda_{\text{em}}^{\text{max}}/\text{nm}$	PLQY/%	$\tau/\mu\text{s}$	PLQY/%
POP	MeObpy	613, 640 <sup>b</sup>	<1	204	565	17	3.3	599	5	21	4
	EtObpy	613, 641 <sup>c</sup>	<1	253	570	9	2.7	596	6	28	5
	PhObpy	610, 641 <sup>d</sup>	1	277	585	5	1.5 <sup>b</sup>	613	3	16	5
	MeSbpy	613, 639 <sup>b</sup>	<1	334	549	30	10.2	563	10	48	5
	EtSbpy	605, 635 <sup>b</sup>	<1	259	564	22	6.5	598	9	31	5
	PhSbpy	606, 630 <sup>e</sup>	<1	258	566	20	6.2	600	7	33	7
	bpy <sup>f</sup>	618, 649	<1	46	580	3	1.5	610	6	16	—
Xantphos	MeObpy	609, 637 <sup>e</sup>	<1	231	566	19	4.7	593	11	23	6
	EtObpy	610, 633 <sup>d</sup>	1	279	566	22	4.0	594	15	23	7
	PhObpy	608, 635 <sup>b</sup>	<1	313	572	12	2.7	610	11	13	6
	MeSbpy	608, 632 <sup>b</sup>	1	315	557	21	6.0	588	20	38	5
	EtSbpy	605, 630 <sup>b</sup>	<1	280	552	32	6.5	575	20	38	6
	PhSbpy	603, 629 <sup>b</sup>	1	303	552	38	9.1	576	23	44	7
	bpy <sup>f</sup>	620, 650	<1	104	587	2	1.3	613	3	11	—

<sup>a</sup>  $\lambda_{\text{exc}} = 365 \text{ nm}$ . <sup>b</sup>  $\lambda_{\text{exc}} = 420 \text{ nm}$ . <sup>c</sup>  $\lambda_{\text{exc}} = 400 \text{ nm}$ . <sup>d</sup>  $\lambda_{\text{exc}} = 410 \text{ nm}$ . <sup>e</sup>  $\lambda_{\text{exc}} = 390 \text{ nm}$ . <sup>f</sup> Data from ref. 69.

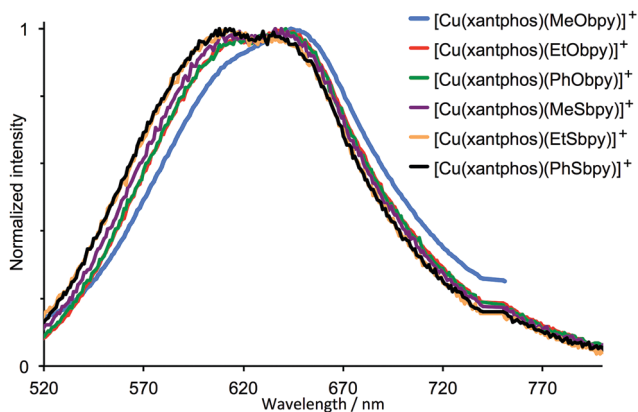


Fig. 5 Emission spectra of solutions ( $\text{CH}_2\text{Cl}_2$ ,  $2.5 \times 10^{-5} \text{ mol dm}^{-3}$ ) of  $[\text{Cu}(\text{xantphos})(\text{N}^{\wedge}\text{N})][\text{PF}_6]$  complexes (see Table 6 for  $\lambda_{\text{exc}}$ ).

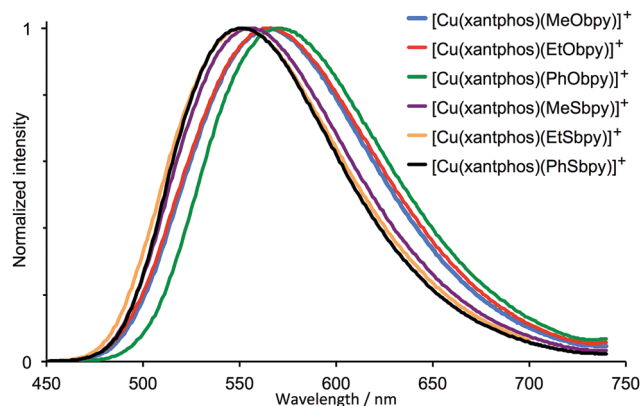


Fig. 6 Emission spectra of powder samples of  $[\text{Cu}(\text{xantphos})(\text{N}^{\wedge}\text{N})][\text{PF}_6]$  complexes ( $\lambda_{\text{exc}} = 365 \text{ nm}$ ).

$[\text{Cu}(\text{POP})(\text{Mebpy})][\text{PF}_6]$ <sup>16</sup> and  $[\text{Cu}(\text{xantphos})(\text{Mebpy})][\text{PF}_6]$ <sup>17</sup> and are blue-shifted with respect to emission maxima of  $[\text{Cu}(\text{POP})(\text{bpy})][\text{PF}_6]$  and  $[\text{Cu}(\text{xantphos})(\text{bpy})][\text{PF}_6]$ .<sup>69</sup> Across the series of compounds, there is some variation in the relative intensities of the two emission bands. This is most noticeable for  $[\text{Cu}(\text{xantphos})(\text{MeObpy})][\text{PF}_6]$  (blue curve in Fig. 5) and  $[\text{Cu}(\text{POP})(\text{MeObpy})][\text{PF}_6]$  (Fig. S27, ESI<sup>†</sup>) where the high energy band is less intense. The PL lifetimes in solution for the series of compounds are relatively short (between 204 and 334 ns), with no evident influence of the P<sup>^</sup>P ligands. We have previously observed that the introduction of the 6-substituents on the bpy results in a longer lifetime<sup>16,17,69</sup> (Table 6), and similar trends are observed here moving from  $[\text{Cu}(\text{P}^{\wedge}\text{P})(\text{bpy})][\text{PF}_6]$  to  $[\text{Cu}(\text{P}^{\wedge}\text{P})(\text{RObpy})][\text{PF}_6]$  or  $[\text{Cu}(\text{P}^{\wedge}\text{P})(\text{RSbpy})][\text{PF}_6]$ .

The PL spectra for the powders are broad and, for each complex, a single maximum is observed (Fig. 6 and Fig. S28, ESI<sup>†</sup>). Moving from solution to solid, the emissions are consistently blue-shifted<sup>17</sup> (Table 6). At the same time, the PLQY is substantially enhanced and longer PL lifetimes  $\tau$  are observed. In general,  $[\text{Cu}(\text{P}^{\wedge}\text{P})(\text{N}^{\wedge}\text{N})][\text{PF}_6]$  complexes with xantphos have

higher PLQYs as compared with POP-based compounds. This is most likely due to the more rigid structure of the xantphos ligand, partially hindering the planarization of the complex in the excited state as discussed above. At the same time, the PLQYs of the complexes bearing the RSbpy ligands are higher than those obtained for the complexes with RObpy ligands. Also, within each class of compounds, the PLQY increases when the size of the 6-substituent on the bpy is augmented, *i.e.* going from MeXbpy to EtXbpy and to PhXbpy (X = O and S). We propose that with the larger substituents, the copper centre is better protected against quenchers such as oxygen or water. Hence, the highest PLQY (38%) is observed for  $[\text{Cu}(\text{xantphos})(\text{PhSbpy})][\text{PF}_6]$ , which is comparable to the best-in-class  $[\text{Cu}(\text{P}^{\wedge}\text{P})(\text{N}^{\wedge}\text{N})][\text{PF}_6]$  complexes (N<sup>^</sup>N = 6-Mebpy, 6,6'-Mebpy) reported to date.<sup>16,17</sup>

As mentioned above, TD-DFT calculations predict that the emitting HOMO  $\rightarrow$  LUMO T<sub>1</sub> triplet has an MLCT character and implies a charge transfer from the Cu(P<sup>^</sup>P) domain, where the HOMO lies, to the bpy ligand, where the LUMO is located (Fig. S25, ESI<sup>†</sup>). As the flattening of the tetrahedral structure of

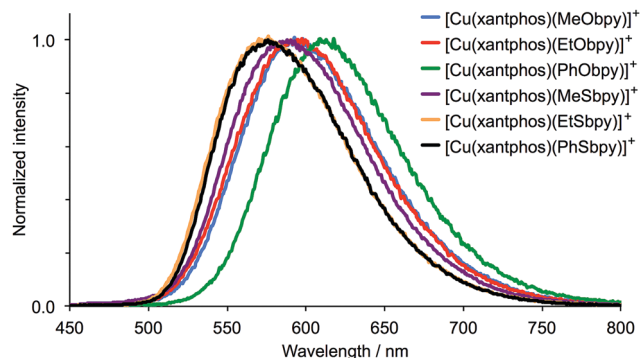


Fig. 7 Emission spectra of  $[\text{Cu}(\text{xantphos})(\text{N}^{\wedge}\text{N})][\text{PF}_6]$  complexes in frozen Me-THF ( $\lambda_{\text{exc}} = 410 \text{ nm}$ ).

the complex in the  $T_1$  state occurs to a similar extent for all the complexes (see Table 3), similar energies in the 1.8–1.9 eV range are predicted for  $T_1$  after full relaxation of the molecular geometry. The close energies calculated for  $T_1$  both at the TD-DFT level (Table 5), determined by the similar HOMO–LUMO gaps, and after full geometry relaxation explain the similarity of the experimentally observed emission maxima (Table 6).

Low temperature emission spectra were recorded for frozen (77 K) solutions of the complexes in Me-THF. The emission spectra of the  $[\text{Cu}(\text{xantphos})(\text{N}^{\wedge}\text{N})][\text{PF}_6]$  and  $[\text{Cu}(\text{POP})(\text{N}^{\wedge}\text{N})][\text{PF}_6]$  compounds are shown in Fig. 7 and Fig. S29 (ESI<sup>†</sup>), respectively. Values of  $\lambda_{\text{em}}^{\text{max}}$ , lifetimes and PLQYs are given in Table 6. The frozen solution approaches the solid state, with PLQYs being intermediate between values observed in solution and in powder. Comparison of PL maxima reveals a bathochromic shift of between 14 and 34 nm when going from powder to frozen Me-THF. The excited state lifetimes increase, which might suggest the presence of TADF<sup>37,38</sup> for these compounds. At room temperature, there is emission from the singlet  $S_1$  state after thermal population from the long-lived triplet excited state  $T_1$ . At 77 K, TADF is less likely to occur and, as a result, the PL is dominated by phosphorescence from  $T_1$  rather than fluorescence from  $S_1$ . The former occurs at lower energies and explains the red-shift of the emission maxima at 77 K. As observed for the solid state, the sulfur-containing compounds exhibit longer lifetimes and higher PLQY values as compared to their oxygen-containing analogues. The energy difference between the  $S_1$  and  $T_1$  states is predicted in the range 0.22–0.25 eV at the optimized geometry of  $S_0$  (Table 4), which is small enough to allow efficient TADF.<sup>37,38</sup> To confirm this prediction, the geometries of the  $S_1$  and  $T_1$  states were further optimized at the TD-DFT level for selected complexes. After full relaxation, the energy difference between  $S_1$  and  $T_1$  is 0.23 eV for  $[\text{Cu}(\text{POP})(\text{MeObpy})]^+$ , 0.21 eV for  $[\text{Cu}(\text{POP})(\text{MeSbpy})]^+$  and 0.21 eV for  $[\text{Cu}(\text{xantphos})(\text{MeSbpy})]^+$ . These energies are slightly smaller than the values obtained from the vertical excitation energies, and support the feasibility of TADF in these systems.

## LECs

The series of compounds was tested in LECs using ITO/PEDOT:PSS as the anode, an emitting layer consisting of the

Table 7 Main device parameters obtained from LECs driven at  $50 \text{ A m}^{-2}$

P <sup>^</sup> P	N <sup>^</sup> N	$t_{\text{on}}/\text{h}$	$\text{Lum}_{\text{max}}/\text{cd m}^{-2}$	$t_{1/2}/\text{h}$	$\text{Eff.}/\text{cd A}^{-1}$
Xantphos	MeObpy	4.2	45	48	0.9
	EtObpy	0.5	79	54	1.6
	PhObpy	1.8	80	47	1.6
	MeSbpy	0.9	44	20	0.9
	EtSbpy	0.7	39	14	0.8
	PhSbpy	3.1	56	80	1.1
	6-Etbpy <sup>a</sup>	0.7	77	51	1.5
POP	MeObpy	15.9	17	200	0.3
	EtObpy	1.0	63	102	1.3
	PhObpy	3.4	37	104	0.7
	MeSbpy	0.4	32	14	0.6
	EtSbpy	0.3	14	6	0.2
	PhSbpy	3.9	22	60	0.4
	6-Etbpy <sup>a</sup>	4.3	53	82	1.1

<sup>a</sup> Data from ref. 17.

complex in the presence of  $[\text{Emim}][\text{PF}_6]$  (4 : 1 molar ratio) and an aluminium cathode. Devices were driven with a pulsed current ( $50 \text{ A m}^{-2}$  average, 50% duty cycle, 1 kHz) and the electroluminescence and voltage were monitored over time. The main device parameters obtained for the entire samples series are reported in Table 7.

The time evolution of efficacy and luminance for devices employing RObpy emitters are reported in Fig. 8, while the data for RSbpy compounds can be found in Fig. S30 (ESI<sup>†</sup>). The evolution of the voltage with time for the complete device series is reported in Fig. S31 (ESI<sup>†</sup>). The spectral shape and position of the electroluminescence (EL) signals were found to be extremely similar for the entire series of materials, independent of the choice of P<sup>^</sup>P and N<sup>^</sup>N ligands (Fig. S32, ESI<sup>†</sup>). The EL maxima are asymmetric with maximum intensities at 585 nm, and can be approximated well with the sum of two Gaussian functions centred at 575 nm and 639 nm (Fig. S33, ESI<sup>†</sup>). Interestingly, these wavelengths are very similar to the PL maxima observed for the series of complexes in the solid state and in solution, respectively.

LECs employing xantphos-based complexes were found to be generally more efficient than the POP analogues, in agreement with the PLQY trend described above for samples in powder. However, the trends in device lifetimes are the reverse. For the complexes with 6-OR substituents on the bpy, the devices containing  $[\text{Cu}(\text{POP})(\text{N}^{\wedge}\text{N})]^+$  exhibit longer lifetimes than those with  $[\text{Cu}(\text{xantphos})(\text{N}^{\wedge}\text{N})]^+$ , whereas for the SR analogues, the device lifetimes are longer for the  $[\text{Cu}(\text{xantphos})(\text{N}^{\wedge}\text{N})]^+$  complexes. We must note, however, that the brightest and more efficient LECs were obtained for complexes including alkoxy-bpy ligands, which showed in general a lower PLQY compared to the alkylthio-derivatives. Within each family of compounds, we also observed (with few exceptions) that the maximum luminance and hence the efficiency increase with increasing steric hindrance of the substituent on the bpy domain, which is probably due to a better stabilization of the tetrahedral complex geometry. We have obtained the brightest and most efficient devices with  $[\text{Cu}(\text{xantphos})(\text{N}^{\wedge}\text{N})][\text{PF}_6]$  with N<sup>^</sup>N = EtObpy and PhObpy; these LECs have similar performances of around  $80 \text{ cd m}^{-2}$

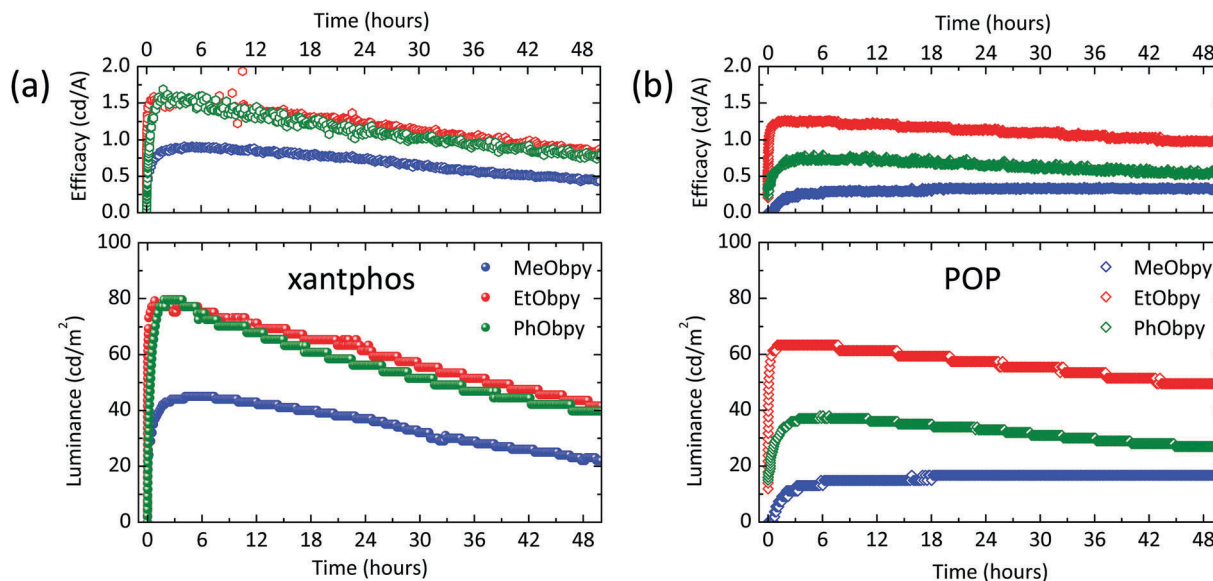


Fig. 8 Efficacy (top) and luminance (bottom) versus time for LECs employing Cu(I) complexes with RObpy and either (a) xantphos or (b) POP ligands. LECs were driven at an average current density of 50 A m<sup>-2</sup>.

and 1.6 cd A<sup>-1</sup> (Fig. 8a). For comparison, the optoelectronic parameters of complexes with 6-Etbp are included in Table 7. On going from [Cu(P<sup>∧</sup>P)(Etbp)] [PF<sub>6</sub>]<sup>17</sup> to [Cu(P<sup>∧</sup>P)(EtObpy)] [PF<sub>6</sub>], whereas there is no substantial difference among xantphos complexes, there is a slight enhancement of the LEC parameters for compounds involving POP. The turn-on time ( $t_{\text{on}}$ , defined here as the time to reach the maximum luminance) shortens from 4.3 to 1.0 h. Lum<sub>max</sub> increases from 53 to 63 cd m<sup>-2</sup>, the device lifetime  $t_{1/2}$  goes from 82 to 102 h, and efficacy from 1.1 to 1.3 cd A<sup>-1</sup>, respectively. The next best complexes are those with a PhO substituent. Interestingly, whereas [Cu(POP)(MeObpy)] [PF<sub>6</sub>] gave the longest device lifetime (> 200 h, Fig. 8b), it came at the expense of  $t_{\text{on}}$  (15.9 h) and the efficacy (0.3 cd A<sup>-1</sup>), with the device only reaching a brightness of 17 cd m<sup>-2</sup>. This is in agreement with our earlier observations that there is a trade-off between brightness and device lifetimes.<sup>17</sup> However, the introduction of the EtO or PhO substituents leads to improved device parameters with respect to the best of our previously reported LECs.<sup>17</sup>

## Conclusions

We have prepared and fully characterized a series of twelve [Cu(P<sup>∧</sup>P)(N<sup>∧</sup>N)] [PF<sub>6</sub>] complexes with a bisphosphane ligand P<sup>∧</sup>P = POP or xantphos and chelating ligand N<sup>∧</sup>N = MeObpy, EtObpy, PhObpy, MeSbpy, EtSbpy or PhSbpy. The single crystal structure of each compound confirms chelating modes for each N<sup>∧</sup>N and P<sup>∧</sup>P ligand, and a distorted tetrahedral geometry for copper(I). The xantphos-containing compounds all exhibit face-to-face  $\pi$ -stacking between phenyl rings of two PPh<sub>2</sub> units. In contrast, intramolecular  $\pi$ -stacking in the POP-containing compounds does not show a consistent pattern. In the xantphos-containing complexes, the asymmetrical bpy ligand is oriented with the 6-OR or SR substituent lying over the xanthene 'bowl'. The compounds are yellow emitters and powder samples show

PLQY values up to 38%, with emission lifetimes  $\leq 10.2$   $\mu$ s. All the compounds have been tested in LECs. Bright and stable LECs are obtained with complexes containing alkoxy- or phenoxy-substituted ligands. Compared with the state-of-the-art copper(I)-based LECs which contain [Cu(P<sup>∧</sup>P)(Etbp)] [PF<sub>6</sub>]<sup>17</sup> the LECs with [Cu(P<sup>∧</sup>P)(EtObpy)] [PF<sub>6</sub>] exhibit enhanced values of  $t_{\text{on}}$ , Lum<sub>max</sub>,  $t_{1/2}$  and efficacy. These observations point towards [Cu(P<sup>∧</sup>P)(N<sup>∧</sup>N)] [PF<sub>6</sub>] compounds with N<sup>∧</sup>N being 6-alkoxy- or 6-phenoxy-bpy ligands being very relevant for the future development of copper-based electroluminescent devices.

## Conflicts of interest

There are no conflicts to declare.

## Acknowledgements

Financial support from the Swiss National Science Foundation (grant number 162631), the University of Basel, the Spanish Ministry of Economy and Competitiveness (MINECO, CTQ2015-71154-P, MAT2017-88821-R, PCIN-2015-255, PCIN-2017-014 and Unidad de Excelencia María de Maeztu MDM-2015-0538), the Generalitat Valenciana (PROMETEO/2016/135), and European FEDER funds (CTQ2015-71154-P) is gratefully acknowledged. M. S. thanks the MINECO for his RyC contract. Fabian Brunner is acknowledged for valuable laboratory assistance. Prof. Oliver S. Wenger is thanked for use of the LP920-KS instrument from Edinburgh Instruments.

## References

- 1 R. D. Costa, E. Ortí, H. J. Bolink, F. Monti, G. Accorsi and N. Armaroli, *Angew. Chem., Int. Ed.*, 2012, **51**, 8178.

- 2 Q. Pei, G. Yu, C. Zhang, Y. Yang and A. J. Heeger, *Science*, 1995, **269**, 1086.
- 3 S. B. Meier, D. Tordera, A. Pertegás, C. Roldán-Carmona, E. Ortí and H. J. Bolink, *Mater. Today*, 2014, **17**, 217.
- 4 Y. Zhang and J. Gao, *J. Appl. Phys.*, 2006, **100**, 084501.
- 5 N. Kaihovirta, C. Larsen and L. Edman, *ACS Appl. Mater. Interfaces*, 2014, **6**, 2940.
- 6 S. Tang, W.-Y. Tan, X.-H. Zhu and L. Edman, *Chem. Commun.*, 2013, **49**, 4926.
- 7 M. D. Weber, M. Adam, R. R. Tykwinski and R. D. Costa, *Adv. Funct. Mater.*, 2015, **25**, 5066.
- 8 M. Y. Wong, G. J. Hedley, G. Xie, L. S. Kolln, I. D. W. Samuel, A. Pertegás, H. J. Bolink and E. Zysman-Colman, *Chem. Mater.*, 2015, **27**, 6535.
- 9 J. D. Slinker, A. A. Gorodetsky, M. S. Lowry, J. Wang, S. Parker, R. Rohl, S. Bernhard and G. G. Malliaras, *J. Am. Chem. Soc.*, 2004, **126**, 2763.
- 10 J.-K. Lee, D. S. Yoo, E. S. Handy and M. F. Rubner, *Appl. Phys. Lett.*, 1996, **69**, 1686.
- 11 F. G. Gao and A. J. Bard, *J. Am. Chem. Soc.*, 2000, **122**, 7426.
- 12 C. E. Housecroft and E. C. Constable, *Coord. Chem. Rev.*, 2017, **350**, 155.
- 13 T. Hu, L. He, L. Duan and Y. Qiu, *J. Mater. Chem.*, 2012, **22**, 4206.
- 14 See for example: C. E. Housecroft and E. C. Constable, *Chem. Soc. Rev.*, 2015, **44**, 8386.
- 15 R. D. Costa, D. Tordera, E. Ortí, H. J. Bolink, J. Schönle, S. Graber, C. E. Housecroft, E. C. Constable and J. A. Zampese, *J. Mater. Chem.*, 2011, **21**, 16108.
- 16 S. Keller, E. C. Constable, C. E. Housecroft, M. Neuburger, A. Prescimone, G. Longo, A. Pertegás, M. Sessolo and H. J. Bolink, *Dalton Trans.*, 2014, **43**, 16593.
- 17 S. Keller, A. Pertegás, G. Longo, L. Martínez, J. Cerdá, J. M. Junquera-Hernández, A. Prescimone, E. C. Constable, C. E. Housecroft, E. Ortí and H. J. Bolink, *J. Mater. Chem. C*, 2016, **4**, 3857.
- 18 F. Brunner, L. Martínez-Sarti, S. Keller, A. Pertegás, A. Prescimone, E. C. Constable, H. J. Bolink and C. E. Housecroft, *Dalton Trans.*, 2016, **45**, 15180.
- 19 A. Kaeser, O. Moudam, G. Accorsi, I. Ségy, J. Navarro, A. Belbakra, C. Duhayon, N. Armaroli, B. Delavaux-Nicot and J.-F. Nierengarten, *Eur. J. Inorg. Chem.*, 2014, 1345.
- 20 C. Bizzarri, C. Strabler, J. Prock, B. Trettenbrein, M. Ruggenthaler, C.-H. Yang, F. Polo, A. Iordache, P. Brüggeller and L. De Cola, *Inorg. Chem.*, 2014, **53**, 10944.
- 21 D. Volz, M. Wallesch, S. L. Grage, J. Göttlicher, R. Steininger, D. Batchelor, T. Vitova, A. S. Ulrich, C. Heske, L. Weinhardt, T. Baumann and S. Bräse, *Inorg. Chem.*, 2014, **53**, 7837.
- 22 J.-J. Cid, J. Mohanraj, M. Mohankumar, M. Holler, F. Monti, G. Accorsi, L. Karmazin-Brelot, I. Nierengarten, J. M. Malicka, M. Cocchi, B. Delavaux-Nicot, N. Armaroli and J.-F. Nierengarten, *Polyhedron*, 2014, **82**, 158.
- 23 N. Armaroli, G. Accorsi, M. Holler, O. Moudam, J. F. Nierengarten, Z. Zhou, R. T. Wegh and R. Welter, *Adv. Mater.*, 2006, **18**, 1313.
- 24 R. Czerwieńiec and H. Yersin, *Inorg. Chem.*, 2015, **54**, 4322.
- 25 K. Zhang and D. Zhang, *Spectrochim. Acta, Part A*, 2014, **124**, 341.
- 26 L. Bergmann, J. Friedrichs, M. Mydlak, T. Baumann, M. Nieger and S. Bräse, *Chem. Commun.*, 2013, **49**, 6501.
- 27 E. Mejía, S.-P. Luo, M. Karnahl, A. Friedrich, S. Tschierlei, A.-E. Surkus, H. Junge, S. Gladiali, S. Lochbrunner and M. Beller, *Chem. – Eur. J.*, 2013, **19**, 15972.
- 28 X.-L. Chen, R. Yu, Q.-K. Zhang, L.-J. Zhou, X.-Y. Wu, Q. Zhang and C.-Z. Lu, *Chem. Mater.*, 2013, **25**, 3910.
- 29 A. Kaeser, M. Mohankumar, J. Mohanraj, F. Monti, M. Holler, J.-J. Cid, O. Moudam, I. Nierengarten, L. Karmazin-Brelot, C. Duhayon, B. Delavaux-Nicot, N. Armaroli and J.-F. Nierengarten, *Inorg. Chem.*, 2013, **52**, 12140.
- 30 C. Femoni, S. Muzzioli, A. Palazzi, S. Stagni, S. Zacchini, F. Monti, G. Accorsi, M. Bolognesi, N. Armaroli, M. Massi, G. Valenti and M. Marcaccio, *Dalton Trans.*, 2013, **42**, 997.
- 31 I. Andrés-Tomé, J. Fyson, F. Baiao Dias, A. P. Monkman, G. Iacobellis and P. Coppo, *Dalton Trans.*, 2012, **41**, 8669.
- 32 C. L. Linfoot, M. J. Leidl, P. Richardson, A. F. Rausch, O. Chepelin, F. J. White, H. Yersin and N. Robertson, *Inorg. Chem.*, 2014, **53**, 10854.
- 33 S.-M. Kuang, D. G. Cuttall, D. R. McMillin, P. E. Fanwick and R. A. Walton, *Inorg. Chem.*, 2002, **41**, 3313.
- 34 K. Chen, J. Shearer and V. J. Catalano, *Inorg. Chem.*, 2015, **54**, 6245.
- 35 M. D. Weber, C. Garino, G. Volpi, E. Casamassa, M. Milanese, C. Barolo and R. D. Costa, *Dalton Trans.*, 2016, **45**, 8984.
- 36 C. L. Linfoot, M. J. Leidl, P. Richardson, A. F. Rausch, O. Chepelin, F. J. White, H. Yersin and N. Robertson, *Inorg. Chem.*, 2014, **53**, 10854.
- 37 R. Czerwieńiec, M. J. Leidl, H. H. H. Homeier and H. Yersin, *Coord. Chem. Rev.*, 2016, **325**, 2.
- 38 *Highly Efficient OLEDs: Materials Based on Thermally Activated Delayed Fluorescence*, ed. H. Yersin, Wiley-VCH, Weinheim, 2018.
- 39 D. G. Cuttall, S.-M. Kuang, P. E. Fanwick, D. R. McMillin and R. A. Walton, *J. Am. Chem. Soc.*, 2002, **124**, 6.
- 40 D. Tordera, S. Meier, M. Lenes, R. D. Costa, E. Ortí, W. Sarfert and H. J. Bolink, *Adv. Mater.*, 2012, **24**, 897.
- 41 N. M. Shavaleev, R. Scopelliti, M. Grätzel, M. K. Nazeeruddin, A. Pertegás, C. Roldan-Carmona, D. Tordera and H. J. Bolink, *J. Mater. Chem. C*, 2013, **1**, 2241.
- 42 F. Brunner, S. Graber, Y. Baumgartner, D. Häussinger, A. Prescimone, E. C. Constable and C. E. Housecroft, *Dalton Trans.*, 2017, **46**, 6379.
- 43 M. D. Weber, M. Viciano-Chumillas, D. Armentano, J. Cano and R. D. Costa, *Dalton Trans.*, 2017, **46**, 6312.
- 44 G. J. Kubas, *Inorg. Synth.*, 1979, **19**, 90.
- 45 *APEX2, version 2 User Manual, M86-E01078*, Bruker Analytical X-ray Systems, Inc., Madison, WI, 2006.
- 46 P. W. Betteridge, J. R. Carruthers, R. I. Cooper, K. Prout and D. J. Watkin, *J. Appl. Crystallogr.*, 2003, **36**, 1487.
- 47 I. J. Bruno, J. C. Cole, P. R. Edgington, M. K. Kessler, C. F. Macrae, P. McCabe, J. Pearson and R. Taylor, *Acta Crystallogr., Sect. B: Struct. Sci.*, 2002, **58**, 389.

- 48 C. F. Macrae, I. J. Bruno, J. A. Chisholm, P. R. Edgington, P. McCabe, E. Pidcock, L. Rodriguez-Monge, R. Taylor, J. van de Streek and P. A. Wood, *J. Appl. Crystallogr.*, 2008, **41**, 466.
- 49 A. L. Spek, *Acta Crystallogr., Sect. C: Struct. Chem.*, 2015, **C71**, 9.
- 50 M. J. Frisch, G. W. Trucks, H. B. Schlegel, G. E. Scuseria, M. A. Robb, J. R. Cheeseman, G. Scalmani, V. Barone, G. A. Petersson, H. Nakatsuji, X. Li, M. Caricato, A. V. Marenich, J. Bloino, B. G. Janesko, R. Gomperts, B. Mennucci, H. P. Hratchian, J. V. Ortiz, A. F. Izmaylov, J. L. Sonnenberg, D. Williams-Young, F. Ding, F. Lipparini, F. Egidi, J. Goings, B. Peng, A. Petrone, T. Henderson, D. Ranasinghe, V. G. Zakrzewski, J. Gao, N. Rega, G. Zheng, W. Liang, M. Hada, M. Ehara, K. Toyota, R. Fukuda, J. Hasegawa, M. Ishida, T. Nakajima, Y. Honda, O. Kitao, H. Nakai, T. Vreven, K. Throssell, J. A. Montgomery Jr., J. E. Peralta, F. Ogliaro, M. J. Bearpark, J. J. Heyd, E. N. Brothers, K. N. Kudin, V. N. Staroverov, T. A. Keith, R. Kobayashi, J. Normand, K. Raghavachari, A. P. Rendell, J. C. Burant, S. S. Iyengar, J. Tomasi, M. Cossi, J. M. Millam, M. Klene, C. Adamo, R. Cammi, J. W. Ochterski, R. L. Martin, K. Morokuma, O. Farkas, J. B. Foresman and D. J. Fox, *Gaussian 16, Revision A.03*, Gaussian, Inc., Wallingford CT, 2016.
- 51 C. Lee, W. Yang and R. G. Parr, *Phys. Rev. B: Condens. Matter Mater. Phys.*, 1988, **37**, 785.
- 52 A. D. Becke, *J. Chem. Phys.*, 1993, **98**, 5648.
- 53 F. Weigend and R. Ahlrichs, *Phys. Chem. Chem. Phys.*, 2005, **7**, 3297.
- 54 F. Weigend, *Phys. Chem. Chem. Phys.*, 2006, **8**, 1057.
- 55 S. Grimme, J. Antony, S. Ehrlich and H. Krieg, *J. Chem. Phys.*, 2010, **132**, 154104.
- 56 S. Grimme, S. Ehrlich and L. Goerigk, *J. Comput. Chem.*, 2011, **32**, 1456.
- 57 M. Petersilka, U. J. Gossmann and E. K. U. Gross, *Phys. Rev. Lett.*, 1996, **76**, 1212.
- 58 C. Jamorski, M. E. Casida and D. R. Salahub, *J. Chem. Phys.*, 1996, **104**, 5134.
- 59 M. E. Casida, C. Jamorski, K. C. Casida and D. R. Salahub, *J. Chem. Phys.*, 1998, **108**, 4439.
- 60 J. Tomasi and M. Persico, *Chem. Rev.*, 1994, **94**, 2027.
- 61 C. J. Cramer and D. G. Truhlar, in *Solvent Effects and Chemical Reactivity*, ed. O. Tapia and J. Bertrán, Kluwer, 1996, pp. 1–80.
- 62 J. Tomasi, B. Mennucci and R. Cammi, *Chem. Rev.*, 2005, **105**, 2999.
- 63 P. M. Pojer and L. A. Summers, *J. Heterocycl. Chem.*, 1974, **11**, 303.
- 64 S.-H. Kim and R. D. Rieke, *Tetrahedron Lett.*, 2009, **50**, 5329.
- 65 J. F. M. da Silva, A. F. Yepes Pérez and N. P. de Almeida, *Synth. Commun.*, 2015, **45**, 1995.
- 66 P. Gros and Y. Fort, *J. Chem. Soc., Perkin Trans. 1*, 1998, 3515.
- 67 J. Carroll, H. G. Woolard, R. Mroz, C. A. Nason and S. Huo, *Organometallics*, 2016, **35**, 131.
- 68 Y.-Q. Fang and G. S. Hanan, *Synlett*, 2003, 852.
- 69 S. Keller, F. Brunner, J. M. Junquera-Hernández, A. Pertegás, M.-G. La-Placa, A. Prescimone, E. C. Constable, H. J. Bolink, E. Ortí and C. E. Housecroft, *ChemPlusChem*, 2018, **83**, 217.
- 70 C. Janiak, *J. Chem. Soc., Dalton Trans.*, 2000, 3885.
- 71 S. Keller, A. Prescimone, H. Bolink, M. Sessolo, G. Longo, L. Martínez-Sarti, J. M. Junquera-Hernández, E. C. Constable, E. Ortí and C. E. Housecroft, *Dalton Trans.*, 2018, DOI: 10.1039/c8dt01338a.
- 72 S. F. Mason, *J. Chem. Soc.*, 1959, 1253.